Precipitation behavior of Heusler phase (Ni_2AlHf) in multiphase NiAl alloy

C. Y. CUI*, J. T. GUO, H. Q. YE
Institute of Metal Research, Chinese Academy of Sciences, Shenyang 110016, China
E-mail: Cui.chuanyong@nims.go.jp

Published online: 28 March 2006

Precipitation behavior of Heusler phase (Ni_2AlHf) in a directionally solidified (DS) NiAl-28Cr-5Mo-1Hf (at.%) alloy was examined using scanning electron microscope (SEM) and transmission electron microscope (TEM). In the as-cast alloy, the Ni_2AlHf phase generally appeared on the NiAl/Cr(Mo) interface, which degraded the NiAl/Cr(Mo) eutectic structure. In the heat-treated alloy, the density of the intercellular Ni_2AlHf phase was slightly reduced. In addition, the spherical Ni_2AlHf phase precipitated heterogeneously in the NiAl matrix, but the Ni_2AlHf phase did not precipitate in the lamellar Cr(Mo) phase. The precipitation behavior of the Ni_2AlHf phase could be explained in terms of the interfacial energy. A lattice model was also proposed to explain the NiAl↔Ni_2AlHf phase transformation.

1. Introduction

NiAl-base directionally solidified eutectics have shown potential to reach an appropriate balance of high temperature creep strength and room temperature fracture toughness. NiAl with Cr, Mo or Cr(Mo) are two phase eutectics that have been extensively studied [1–3]. These alloys have second phases that improve the fracture toughness by crack deflection and crack bridging [3]. While all these alloys have shown the potential to provide a reasonable balance of creep and toughness properties, higher creep rupture strengths are still needed for aircraft engine applications. Recently, we have tried to improve the strength of the NiAl/Cr(Mo) eutectic through alloying additions, such as Hf and Zr [4–6]. These efforts are based on the earlier works that Hf and other Heusler-forming elements significantly increase the high temperature strength of NiAl [7, 8].

Previous studies showed that the Hf-containing NiAl/Cr(Mo) alloys possess higher yield stress and improved creep strength than the base alloy, NiAl/Cr(Mo) [4–6]. For example, the yield stress of the Hf-containing NiAl/Cr(Mo) alloy is almost 2 times higher than that of NiAl/Cr(Mo) alloy [4]. The creep strength of this alloy at 1100°C is higher than that of Ni-base superalloy Rene 80. Furthermore, the fracture toughness of the Hf-containing NiAl/Cr(Mo) alloy can be also improved by controlling the Hf addition and solidification rate [6]. Unfortunately, the element Hf mainly exists on the NiAl/Cr(Mo) interface in all the Hf-containing NiAl/Cr(Mo) alloys, and thus degrades the eutectic structure, resulting in the lower fracture toughness and creep rupture life. Thus, controlling the morphology and distribution of the Hf-concerning phase are a critical step to attain the better mechanical properties in the Hf-containing NiAl/Cr(Mo) alloys. In the previous study [9], we reported that the hot isostatic pressed NiAl-Cr(Mo)-Hf alloys show the improved yield strength at high temperature, which demonstrates that the strength improvement can be achieved by heat treatment. However, the effect of heat treatment on the precipitation behavior of Ni_2AlHf phase has not been clear yet. Therefore, the purpose of this study is to determine the precipitation behavior of Heusler phase in the Hf-containing NiAl/Cr(Mo) alloy.

2. Experimental procedure

The nominal chemical composition of the alloy used was a Ni-33Al-28Cr-5Mo-1Hf (at.%). The vacuum induction melted and drop cast ingot was directionally solidified

*Author to whom all correspondence should be addressed.
0022-2461
DOI: 10.1007/s10853-006-6732-3

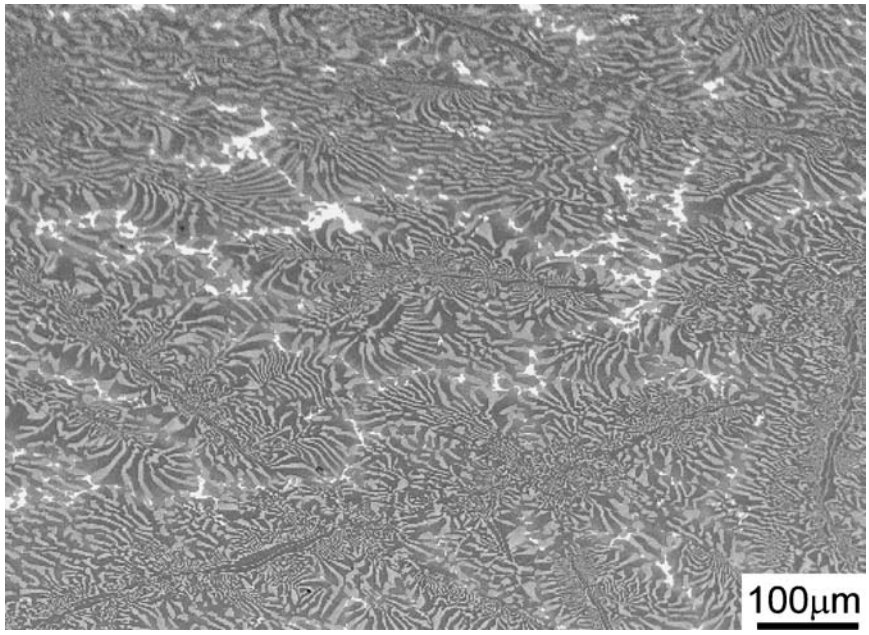

Figure 1 The typical SEM image of the as-cast NiAl-Cr(Mo)-Hf alloy observed along the transverse section. Here, the NiAl matrix showed the dark contrast, the Cr(Mo) phase showed the light gray contrast, the needle-like phase was a Cr(Mo) variant and the Heusler phase showed the white contrast.

(DS) in an Ar atmosphere in the Al_2O_3-SiO_2 ceramic mold. Based on the previous study [10], a homogenization temperature of 1307°C was selected to reduce the intercellular Ni_2AlHf phase and at the same time to avoid the incipient melting of the Ni_2AlHf phase. To determine the effect of heat treatment on the thermal stability of the Ni_2AlHf phase, some samples were heat treated at 1307°C for 40 h and then aged at 1027°C for 20°h. All the samples were observed in a JSM6301F scanning electron microscope (SEM) operated in a back-scatter electron microscope (BSE). Qualitative chemical analyses of the precipitates were performed using an energy dispersive spectrometer (EDS) attached to the SEM. The measurements were the average values of 10 measurements made for each phase. The errors were the standard deviation from the measurements. The volume fraction of the Cr(Mo) phase and Heusler phase was also determined from the 10 images using the software Image-Pro Plus (IPP). The transmission electron microscope (TEM) samples were also prepared by conventional ion-thinning process and were observed in a JEM2010 high resolution electron microscope (HREM).

3. Results

3.1. As-cast alloy

Fig. 1 shows the typical microstructure of the NiAl-Cr(Mo)-Hf alloy along the transverse section. The alloy mainly consisted of the NiAl matrix, the lamellar Cr(Mo) phase, the needle-like phase and the intercellular white phase. The result of the EDS analysis showed the needle-like phase to be enriched in Cr, Mo, Ni and Al, however the actual content of Ni and Al should be much lower than the measured one due to the small size of the particle relative to the probe size. Moreover, the phase showed the similar contrast with the Cr(Mo) phase by BSE observation. Thus, the needle-like phase was identified to be a Cr(Mo) variant, The white phase was identified to be the Heusler phase (Ni_2AlHf) by EDS analysis, as listed in Table I. Thus the Ni_2AlHf phase could be formed with higher Hf addition in the NiAl/Cr(Mo) alloy. The Ni_2AlHf phase mainly distributed on the grain boundary of the NiAl/Cr(Mo) eutectic and rarely observed in the center of the cell. The volume fraction of the Ni_2AlHf phase was analyzed by IPP and the result was approximately 6%. The intercellular Ni_2AlHf phase degraded

TABLE I. Chemical composition of the NiAl and Ni_2AlHf phases in the NiAl-Cr(Mo)-Hf alloy (at.%)

	Ni	Al	Si	Cr	Hf	Mo
NiAl[a]	46.5 ± 0.6	44.8 ± 0.3	–	7.5 ± 0.5	0.4 ± 0.2	0.8 ± 0.1
Ni_2AlHf[a]	48.3 ± 1.4	23.7 ± 0.8	2.6 ± 0.3	3.1 ± 0.5	22.3 ± 1.6	–
NiAl[b]	48.8 ± 1.2	46.9 ± 0.7	0.4 ± 0.1	2.6 ± 0.6	0.9 ± 0.1	0.5 ± 0.2
Ni_2AlHf[b]	48.4 ± 0.8	24.6 ± 1.0	1.6 ± 0.4	2.3 ± 0.3	23.0 ± 1.2	–

[a]represents the as-cast alloy.
[b]represents the heat-treated alloy.

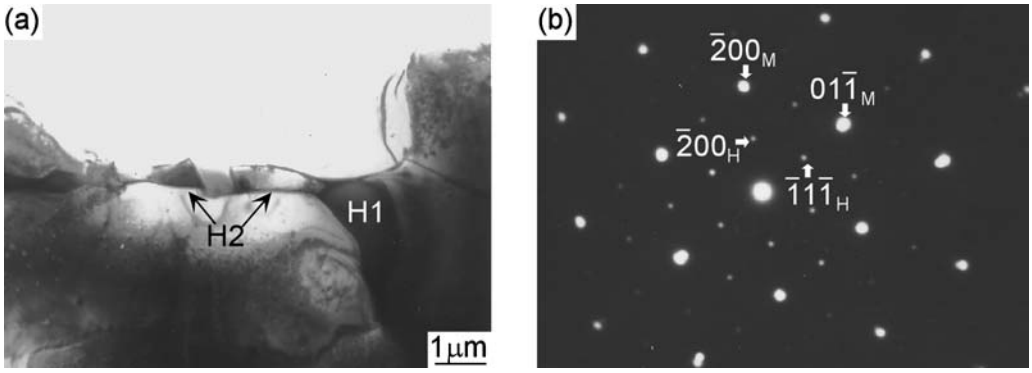

Figure 2 (a) TEM observation of the Ni_2AlHf phase in the as-cast NiAl-Cr(Mo)-Hf alloy (the Ni_2AlHf phases are indicted by H_1 and H_2). (b) EDP taken along the [011] axes of NiAl and H_2.

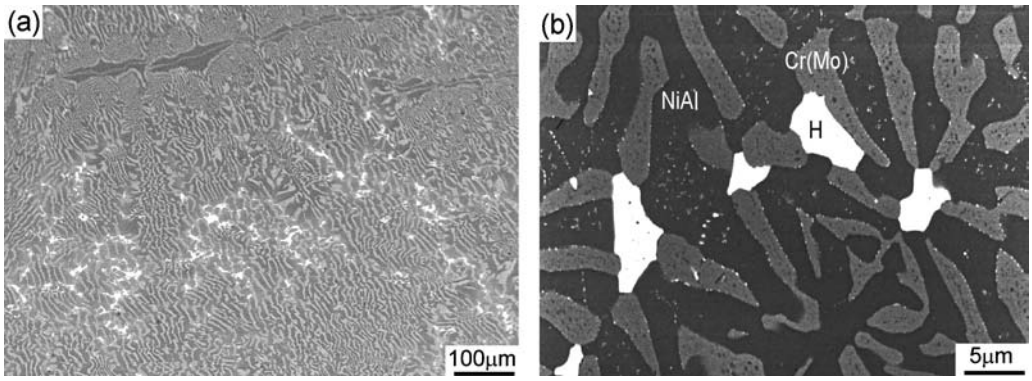

Figure 3 The typical SEM image at low magnification (a) and high magnification (b)of the heat-treated NiAl-Cr(Mo)-Hf alloy observed along the transverse section. H represents the Ni_2AlHf phase.

the eutectic microstructure, resulting in the lower fracture toughness and rupture strength than the base alloy, as we previously reported [4, 6]. The minor phase, $Ni_{16}Hf_6Si_7$, was also found in this alloy because of the Si contamination in the directional solidification process. A detailed description of the formation and thermal stability of the $Ni_{16}Hf_6Si_7$ phase was presented in our previous studies [5, 11].

TEM observation confirmed that the Ni_2AlHf phase mainly appeared on the NiAl/Cr(Mo) interface, but the Ni_2AlHf phases were not observed in the NiAl matrix and lamellar Cr(Mo) phase. Fig. 2 shows the TEM observation of the Ni_2AlHf phase in the NiAl/Cr(Mo) interface. Two types of the Ni_2AlHf phase marked by H_1 and H_2 were found in the as-cast alloy. The blocky Ni_2AlHf phase (H_1) can be easily observed in the samples. Electron diffraction pattern (EDP) analysis showed that there was no orientation relationship between H_1 and NiAl. In some cases, smaller Ni_2AlHf phases were also found, as marked by H_2 in Fig. 2(a). The results of the EDS analysis in the TEM showed that the two types of the Heusler phases had the similar chemical composition, as indicated in Table I. Fig. 2(b) shows the EDP taken along the [011] zone axes of the NiAl and H_2. A cube-on-cube relationship was found between NiAl and H_2, i.e., $\langle 111\rangle_{NiAl}//\langle 111\rangle_H$, $\{10\bar{1}\}_{NiAl}//\{10\bar{1}\}_H$.

3.2. Heat-treated alloy

Fig. 3 shows the typical microstructure of the heat-treated NiAl-Cr(Mo)-Hf alloy along the transverse section. Compared with the as-cast alloy shown in Fig. 1, the density of the intercellular Ni_2AlHf phase was slightly reduced (Fig. 3(a)). In addition, some fine precipitates with bright contrast were also found in the NiAl matrix and on the NiAl/Cr(Mo) interface, as shown in Fig. 3(b). Since the fine precipitates showed the similar bright contrast with the blocky Ni_2AlHf phase, they may be the fine Ni_2AlHf phase. Table I lists the chemical composition of the NiAl and Ni_2AlHf phases. It was clear that the Hf contents in the NiAl matrix increased by the heat treatment, indicating that the partitioning of Hf in the NiAl was also increased.

Fig. 4 shows the TEM observation of the heat-treated NiAl-Cr(Mo)-Hf alloy. As shown in Fig. 4(a), some fine precipitates with 50–100 nm in size were distributed on the NiAl/Cr(Mo) interface. Selected area electron diffraction patterns suggested that the intercellular precipitates were the Ni_2AlHf phase. Grain boundaries of the NiAl matrix provided another precipitation site for the Ni_2AlHf phase, as shown in Fig. 4(b). The spherical Ni_2AlHf phase precipitated around the high density dislocations. Mobile dislocation in the NiAl matrix entangled with these fine Ni_2AlHf particles. Fig. 4(c) shows a TEM bright field

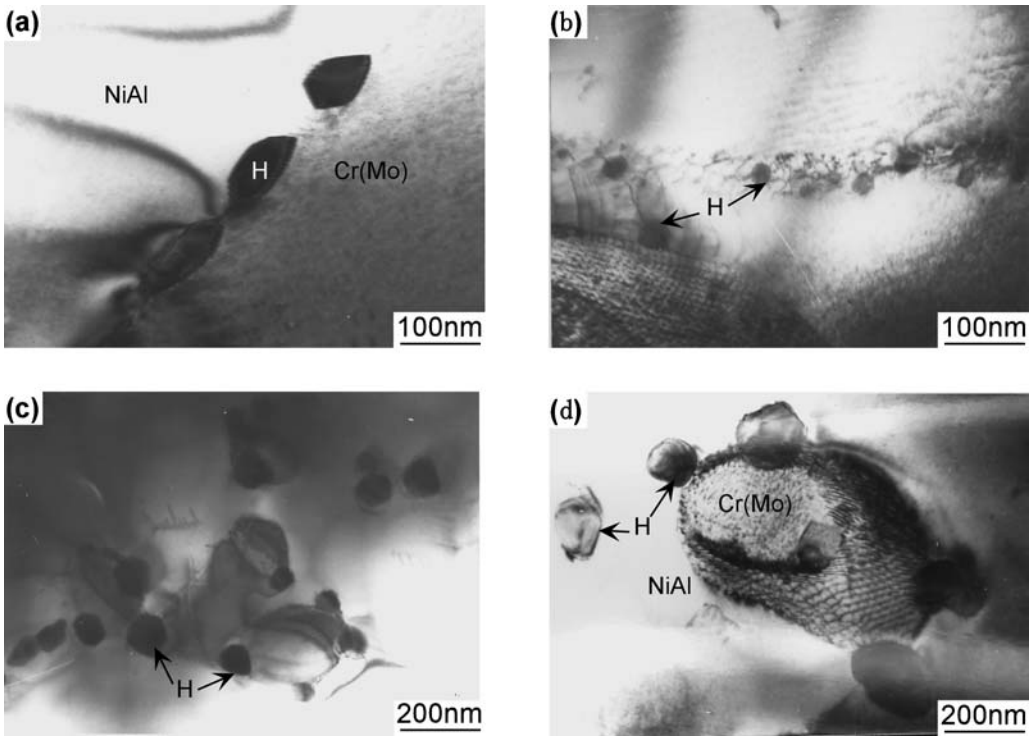

Figure 4 TEM observation on the precipitation behavior of the Ni_2AlHf phase in the heat-treated NiAl-Cr(Mo)-Hf alloy, (a) on the NiAl/Cr(Mo) interface; (b) on the grain boundaries of NiAl; (c) (d) in the NiAl matrix. H represents the Ni_2AlHf phase.

(BF) image of the spherical Ni_2AlHf phase in the NiAl matrix. EDP analysis showed that there was a consistent cube-on-cube orientation relationship between NiAl and Ni_2AlHf. In addition to the lamellar Cr(Mo) phase, the Cr(Mo) precipitates were also found in the NiAl matrix. The NiAl/Cr(Mo) interface was also the nucleation sites for the Ni_2AlHf phase, as shown in Fig. 4(d). It is interesting to find that the Ni_2AlHf phase precipitated in the vicinity of the Cr(Mo) phase, which was never observed in the as-cast alloy. The misfit dislocation between the NiAl and Cr(Mo) was also found in this image, indicating that the fine Ni_2AlHf phase lose its coherency with the NiAl matrix.

From the SEM and TEM observation, the following tendencies for the precipitation behavior of the Ni_2AlHf phase were found: the Ni_2AlHf phase mainly precipitated on the NiAl/Cr(Mo) interface; some amounts of Ni_2AlHf phase were found in the NiAl matrix, either on the grain boundary or in the interior grain. But, no Ni_2AlHf phase was found in the lamellar Cr(Mo) phase. It is noted that all the Ni_2AlHf phase in the NiAl matrix showed the spherical shape, this implied that the shape of the Ni_2AlHf phase could be dominated by the interfacial energy, which will be discussed later.

4. Discussion

4.1. Precipitation behavior of the Ni_2AlHf phase

It is known that the elastic interaction between the misfitting particles affects not only the shape and the coarsening behavior, but also the spatial arrangement. The effect of coherency strain on the shape and spatial arrangement of the precipitates is well established for the γ/γ' system in Ni-base superalloys. Voorhees et al. [12] have derived a dimensionless parameter (L), which defines the relative dominance of strain and interfacial energy on the shape of coherent precipitates in cubic systems. The parameter L is given by

$$L = \delta^2 C_{44} l/\sigma \tag{1}$$

where δ is the dilatational misfit strain, C44 is an element of the cubic symmetric elastic-constant tensor, ι is a characteristic length of the precipitate (equivalent radius), and σ is the isotropic interfacial energy. For small L values, i.e., $L \ll 1$, the interfacial energy dominates the equilibrium shape, giving a spherical morphology; For large L values, i.e., $L \gg 1$, the elastic energy dominates the equilibrium shape, and the resultant shape may vary from cuboidal to plate shape. As shown in Fig. 4(b)–(d), the Ni_2AlHf phase in the NiAl matrix showed the spherical shape in the heat-treated alloy, it is therefore concluded that the interfacial energy dominates the precipitation behavior of Ni_2AlHf phase during heat treatment. Thus, the heterogeneous precipitation behavior of the Ni_2AlHf phase can be explained in terms of the interfacial energy.

Fig. 5 shows an example of the Ni_2AlHf phase appeared on the NiAl/Cr(Mo) interface in the heat-treated alloy. γ, γ_A, and γ_B represent the interfacial energy of

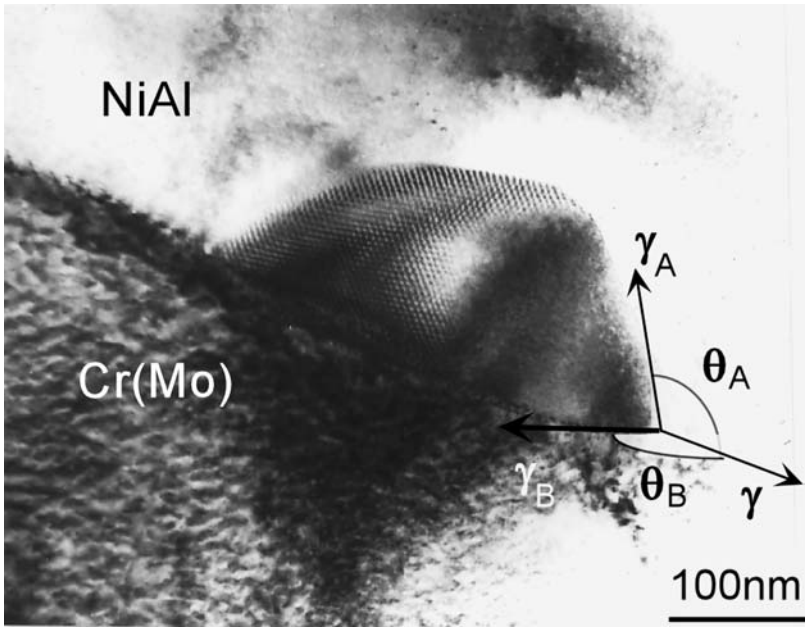

Figure 5 TEM image of a Ni_2AlHf phase precipitated on the NiAl/Cr(Mo) interface.

NiAl/Cr(Mo), NiAl/Ni_2AlHf, and Cr(Mo)/Ni_2AlHf, respectively. The contact angles between γ-γ_A and between γ-γ_B are named as θ_A and θ_B, respectively. Based on the criterion of energy balance, two equations can be obtained:

$$\gamma_A \cos\theta_A + \gamma_B \cos\theta_B + \gamma = 0 \quad (2)$$

$$\gamma_A \sin\theta_A - \gamma_B \sin\theta_B = 0 \quad (3)$$

θ_A and θ_B are measured to 130° and 150°. By using the measured θ_A and θ_B, the following results, $\gamma_B = 1.53\ \gamma_A$, $\gamma = 1.97\ \gamma_A$, can be obtained in spite of the interfacial energy anisotropy.

In the as-cast alloy, the volume fraction of the lamellar Cr(Mo) phase determined by software IPP was about 36%, which provides a large number of precipitation site for the Ni_2AlHf phase. Moreover, as mentioned above, the interfacial energy between NiAl and Cr(Mo) is the highest among the three ($\gamma = 1.97\ \gamma_A$). Therefore, the Ni_2AlHf phases mainly distributed on the NiAl/Cr(Mo) interface, because of a reduction the energy of the whole system. As a result, the intercellular Ni_2AlHf phase in the Hf-containing NiAl/Cr(Mo) alloy is very difficult to eliminate. The Ni_2AlHf phase on the grain boundaries of the NiAl also shows the same tendency. It is apparent that the quantity on the grain boundary is less than that on the NiAl/Cr(Mo) interface, as shown in Fig. 1 and Fig. 3, thus the amounts of the Ni_2AlHf phase existing on the grain boundaries are less than those of the NiAl/Cr(Mo) interface.

According to $\gamma_B = 1.53\ \gamma_A$, the interfacial energy of the Cr(Mo)/Ni_2AlHf is higher than that of the NiAl/Ni_2AlHf. Thus, the Ni_2AlHf phases are less frequently observed in the Cr(Mo) phase than in the NiAl phase, because the precipitation of the Ni_2AlHf phase in the Cr(Mo) phase would lead to higher interfacial energy. In addition, the solid solubility of Hf in Cr is almost zero according to Cr-Hf binary diagram [13], whereas the solid solution limit of Hf in NiAl is reported to be 0.3 at.% [7]. Thus, the nucleation and growth of the Ni_2AlHf phase in the Cr(Mo) phase need a long-range diffusion of Ni, Al and Hf atoms, which makes it more difficulty for the precipitation of the Ni_2AlHf phase in the Cr(Mo) phase.

In the present study, it was found that the Heusler phases nucleated heterogeneously at defects (grain boundary, interface and dislocation). This implied that the driving force for nucleation of the Heusler phase was low and the diffusivity of Hf was high at the aged temperature of 1027°C. The homogenous nucleation of the Heusler phase in the NiAl matrix can be achieved at lower temperature. Similar results were also reported in NiAl-Ti alloys [14].

4.2. NiAl↔Ni_2AlHf transformation

Fig. 6 shows the crystal structure of Ni_2AlHf ($L2_1$) and NiAl (B2) phases. The NiAl is an ordered form of the body-centered cubic (bcc) structure, with the unit cell corner atomic position occupied by Ni atoms, while the body center positions are occupied by Al atoms. The Ni_2AlHf phase is a ternary compound, with a cubic $L2_1$ structure in which the unit cell comprises eight B2-type cells with Al and Hf atoms occupying two sets of octahedral sites located at body center sublattice position [15]. Based on the crystal structure of B2 and $L2_1$, Fig. 6, we proposed a lattice model to explain the NiAl↔Ni_2AlHf phase transformation. For simplicity, this transformation is divided into two steps: (1) the substitution of Hf atom for Al atom, because the element Hf has a strong preference to reside on Al sites in NiAl alloy [16]. As for the

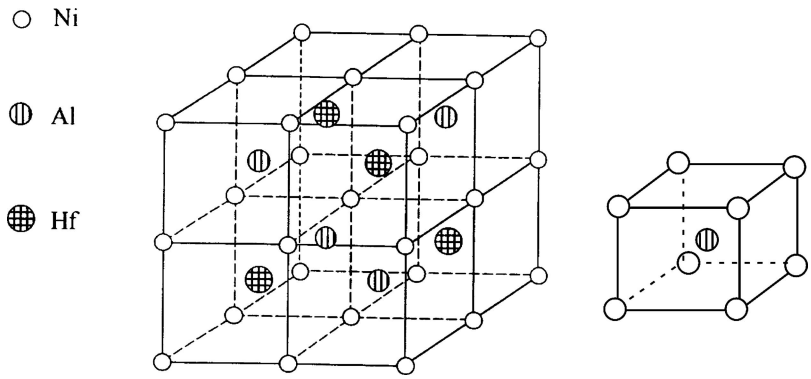

Figure 6 The unit cells of (a) the Ni_2AlHf ($L2_1$) and (b) the NiAl (B2) phases.

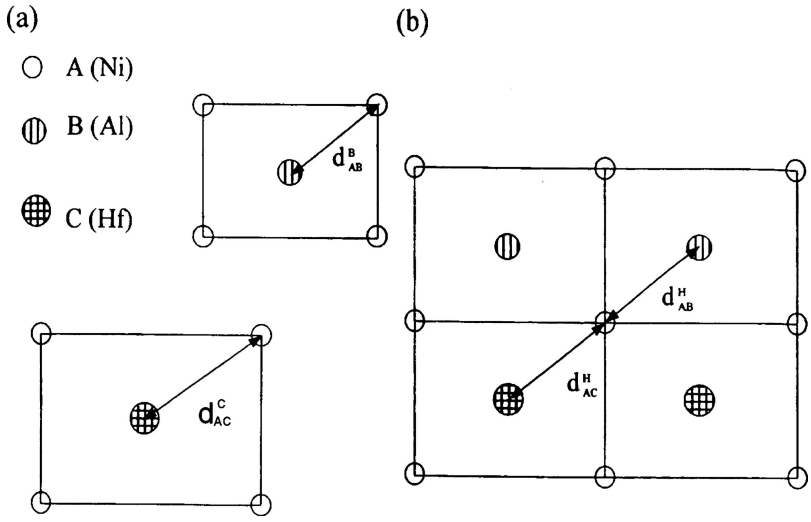

Figure 7 Schematic illustration of (a) B2 structure, NiAl and NiHf compounds, and (b) Ni_2AlHf structure viewing from the {011} close-packed plane.

nucleation of the Ni_2AlHf phase, its stoichiometric must be satisfied locally. We assume that prior to the nucleation of the Ni_2AlHf phase, the Hf atoms, originally fluctuating random on the simple B2-ordered NiAl matrix, begin to distribute locally in an ordered way. When the stoichiometry of the Ni_2AlHf phase is satisfied in a local area, the Hf atoms could substitute for half of the Al atoms. (2) the geometry deformation of two kinds of sublattice, i.e., NiAl and NiHf, to form the crystal lattice of the Ni_2AlHf phase.

Fig. 7 shows a schematic illustration of the B2 and the $L2_1$ lattice viewing from the {011} close-packed plane. As shown in Fig. 7(a), the crystal structure of Ni_2AlHf can be described as a combination of two kinds of B2 sublattice, i.e., NiAl and NiHf after the first step of transformation. In the NiAl sublattice, the atom spacing between Ni and Al, d^A_{AB}, is calculated to 0.250 nm. However there is no B2-structure NiHf alloy reported in the literature. Because the elements Ti and Hf belong to the same column in the periodic table and the NiTi alloy has the B2 structure, the atom spacing between Ni and Hf, d^C_{AC}, can be estimated by the following step: the sum of the Goldschmidt radii of Ni and Hf is multiplied by a correction factor (0.989). The correction factor is obtained from the difference in lattice parameter of NiTi (0.3015 nm) [17] and the values from the Goldschmidt radius (0.3048 nm). We obtained d^C_{AC}= 0.274 nm. The lattice constant of NiHf is 9.6% larger than that of NiAl. In order to maintain the cubic crystal in the Ni_2AlHf phase, d^B_{AB} must be the same as d^C_{AC}, which results in $d^{\mathrm{H}}_{\mathrm{AB}} = d^{\mathrm{H}}_{\mathrm{AC}} = 0.262$ nm. As a result, the NiAl sublattice is considered to be expanded by 4.8%, whereas the NiHf sublattice is contracted by 4.8% when the two B2 sublattices combine into the Ni_2AlHf lattice structure. The lattice misfit between NiAl and Ni_2AlHf was estimated from the electron diffraction pattern shown in Fig. 2(b) to be approximately 4.7%, which is consistent with Takeyama's result [15]. It is interesting to find that the lattice misfit value is close to the expanded value of NiAl sublattice. Thus, the internal "strained lattice" is formed in the Ni_2AlHf lattice, resulting in the brittleness of the Ni_2AlHf phase.

5. Conclusions

1. The as-cast NiAl-Cr(Mo)-Hf alloy mainly consisted of the NiAl matrix, the lamellar Cr(Mo) and the Ni_2AlHf phase. The Ni_2AlHf phase mainly appeared on the NiAl/Cr(Mo) interface.

2. The density of the intercellular Ni_2AlHf phase was slightly reduced by the heat treatment. Some amounts of the Ni_2AlHf phase precipitated in the NiAl matrix. However, the Ni_2AlHf phase did not precipitate in the lamellar Cr(Mo) phase.

3. The precipitation behavior of the Ni_2AlHf phase in the NiAl-Cr(Mo)-Hf alloy was explained in terms of the interfacial energy. It was concluded that the intercellular Ni_2AlHf phase could not be eliminated by heat treatment, because the volume fraction of the lamellar Cr(Mo) was relatively high, and the interfacial energy between NiAl and Cr(Mo) is the highest among the three interfaces.

References

1. J. L. WALTER and H. E. CLINE, *Met. Trans.* **4** (1973) 33.
2. F. E. HEREDIA, M. Y. HE, G. E. LUCAS, A. G. EVANS, H. E. DEVE and D. KONITZER, *Acta. Metall. Mater.* **41**(2) (1993) 505.
3. D. R. JOHNSON, X. F. CHEN, B. F. OLIVER, R. D. NOEBE and J. D. WHITTERBERGER, *Intermetallics*. **3** (1995) 99.
4. J. T. GUO, C. Y. CUI, Y. X. CHEN, D. X. LI and H. Q. YE, *Intermetallics*. **9** (2001) 287.
5. C. Y. CUI, Y. X. CHEN, J. T. GUO, D. X. LI and H. Q. YE, *Mater. Lett*. **43** (2000) 303.
6. C. Y. CUI, J. T. GUO, Y. H. QI and H. Q. YE, *Intermetallics*. **10** (2002) 1001.
7. W. S. WALSTON, R. D. FIELD, J. R. DOBBS, D. F. LAHRMAN and R. DAROLIA, Structural Intermetallics, R. DAROLIA, J. J. LEWANDOWSKI, C. T. LIU, P. L. MARTIN, D. B. MIRACLE and M. V. NATHAL (eds.) (TMS, Warrendale, PA, 1993) p. 523.
8. A. GARG, S. V. RAJ, R. D. NOEBE, M. V. NATHAL and R. DAROLIA, *Metall. Mater. Tran. A.* **29**(1) (1998) 179.
9. C. Y. CUI, J. T. GUO, Y. H. QI and H. Q. YE, *Mater. Lett.* **51**(5) (2001) 444.
10. I. E. LOCCI, R. M. DICKERSON, A. GARG, R. D. NOEBE, J. D. WHITTENBERGER, M. V. NATHAL and R. DAROLIA, *J. Mater. Res.* **11** (1996) 3024.
11. C. Y. CUI, J. T. GUO, Y. H. QI and H. Q. YE, *Metall. Mater. &Trans. A.* **34**(A) (2003) 2663.
12. P. W. VOORHEES, G. B. MCFADDEN and W. C. JOHNSON, *Acta. mater.* **40** (1992) 2979.
13. T. B. MASSALSKI, H. OKAMOTO, P. R. SUBRAMANIAN and L. KACPRZAK, *Binary Alloy Phase Diagrams* 1992, 1281.
14. A. W. WILSON, J. M. HOWE, A. GARG and R. D. NOEBE, *Mater. Sci.&Engin. A.* **289** (2000) 162.
15. M. TAKEYAMA and C. T. LIU, *J. Mater. Res.* **5** (1990) 1189.
16. A. W. WILSON and J. M. HOWE, *Acta. mater.* **49** (2001) 2653.
17. P. VILLARS and L. D. CALVERT, Pearson's Handbook of Crystallographic Data for Intermetallic Phases (American Society for Metals, Metals Park, OH, 1985).

Received 21 May
and accepted 29 August 2005